ACS ES&T Air

pubs.acs.org/estair

Article

Observational Constraints on the Aerosol Optical Depth−Surface $PM_{2.5}$ Relationship during Alaskan Wildfire Seasons

Published as part of ACS ES&T Air virtual special issue "Wildland Fires: Emissions, Chemistry, Contamination, Climate, and Human Health".

Tianlang Zhao,* Jingqiu Mao,* Pawan Gupta, Huanxin Zhang, and Jun Wang

Cite This: *ACS EST Air* 2024, 1, 1164−1176

Read Online

ACCESS | Metrics & More | Article Recommendations | Supporting Information

ABSTRACT: Wildfire is one of the main sources of $PM_{2.5}$ (particulate matter with aerodynamic diameter < 2.5 μm) in the Alaskan summer. The complexity in wildfire smokes, as well as limited coverage of ground measurements, poses a big challenge to estimate surface $PM_{2.5}$ during wildfire season in Alaska. Here we aim at proposing a quick and direct method to estimate surface $PM_{2.5}$ over Alaska, especially in places exposed to strong wildfire events with limited measurements. We compare the AOD−surface $PM_{2.5}$ conversion factor (η = $PM_{2.5}$/AOD; AOD, aerosol optical depth) from the chemical transport model GEOS-Chem (η_{GC}) and from observations (η_{obs}). We show that η_{GC} is biased high compared to η_{obs} under smoky conditions, largely because GEOS-Chem assigns the majority of AOD (67%) within the planetary boundary layer (PBL) when AOD > 1, inconsistent with satellite retrievals from CALIOP. The overestimation in η_{GC} can be to some extent improved by increasing the injection height of wildfire emissions. We constructed a piecewise function for η_{obs} across different AOD ranges based on VIIRS-SNPP AOD and PurpleAir surface $PM_{2.5}$ measurements over Alaska in the 2019 summer and then applied it on VIIRS AOD to derive daily surface $PM_{2.5}$ over continental Alaska in the 2021 and 2022 summers. The derived satellite $PM_{2.5}$ shows a good agreement with corrected PurpleAir $PM_{2.5}$ in Alaska during the 2021 and 2022 summers, suggesting that aerosol vertical distribution likely represents the largest uncertainty in converting AOD to surface $PM_{2.5}$ concentrations. This piecewise function, η'_{obs}, shows the capability of providing an observation-based, quick and direct estimation of daily surface $PM_{2.5}$ over the whole of Alaska during wildfires, without running a 3-D model in real time.

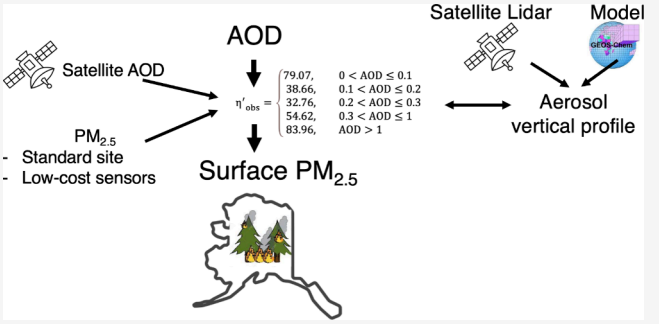

KEYWORDS: *Alaska, wildfire smoke, VIIRS, CALIOP, low-cost sensor, $PM_{2.5}$*

1. INTRODUCTION

Wildfire is one of the major sources for surface $PM_{2.5}$[1−4] and has become a major cause for respiratory diseases and reduction in life expectancy.[5,6] In recent decades, wildfires have shown an increasing trend in the western United States and boreal region,[7−12] and this trend will likely continue. The majority of Alaskan wildfires occur over interior Alaska boreal forest region between the Brooks and Alaska mountain ranges. Alaska's wildfire season usually starts in April and ends in August but has become longer over the past 40 years. The burned area of Alaskan fires has also increased due to more frequent lighting strikes. In Alaska, wildfire has burned 31.4 million acres in the past 20 years, over 2.5 times more than the burned area in the previous two decades. In the 2005, 2009, 2015, and 2019 summers, wildfire burned more than 3 million acres in Alaska, mostly due to lightning-caused fires. As a result, wildfire is now a major threat to the air quality in the Alaskan summer.[13] Currently, there are a limited amount of $PM_{2.5}$ ground measurements in Alaska, making it challenging to estimate air quality, especially that of tribal villages, in Alaskan summer fire seasons.

Satellite AOD has been widely used to derive surface $PM_{2.5}$ in global and regional scales.[14−16] Several satellite AOD products, including Moderate Resolution Imaging Spectroradiometer (MODIS, on board Aqua and Terra) and Multi-angle Imaging Spectro Radiometer (MISR, on board Terra), are extensively used. With these satellites far beyond their life expectancies and facing degradations, the Visible Infrared Imaging Radiometer Suite (VIIRS, on board Suomi National Polar-orbiting Partner-

Received: June 4, 2024
Revised: July 22, 2024
Accepted: July 24, 2024
Published: August 26, 2024

ship (SNPP), NOAA-20 and -21) becomes the new generation polar-orbiting instrument for AOD in the daytime[17] and has the potential to provide nighttime AOD as well for mapping surface $PM_{2.5}$.[18,19] Several statistical methods have been developed to relate satellite columnar AOD to surface $PM_{2.5}$, such as simple linear regression,[14,16] multivariant linear regression,[20−22] geographically weighted regression (GWR),[23−27] and machine learning.[28−30] Another widely used method to derive surface $PM_{2.5}$ is to integrate a chemical transport model (CTM) that provides a conversion factor $\eta = PM_{2.5}/AOD$ or a relationship between $PM_{2.5}$ and top-of-atmosphere radiance; the former can be applied to satellite-based AOD[31−33] while the latter can be applied to satellite-measured radiance.[34,35] In both cases, the spatiotemporal relationship between surface $PM_{2.5}$ and satellite data are accounted for by a CTM. Statistical methods have been more successful where ground measurements are available and at shorter time scales (hourly and daily), whereas the η method is easier for implementation and is mostly used for longer term averages (annually and monthly).

One major challenge of deriving surface $PM_{2.5}$ concentrations with satellite AOD is for extreme events such as wildfire.[36] This is largely due to the unpredictable nature of wildfire emissions as well as the model representation of wildfire plumes. First, wildfire plumes are often injected at various altitudes depending on burning conditions,[37] resulting in a wide range of the AOD−$PM_{2.5}$ relationship due to the diverse vertical distribution of aerosols.[16,32,36] Second, the transport and evolution of wildfire plumes introduces spatial and temporal variability into the relationship between AOD and surface $PM_{2.5}$.[38] As a result, it is difficult to establish a unified AOD−surface $PM_{2.5}$ relationship across time and space. Third, the time scale of wildfire plumes (days) makes it difficult to establish a constant AOD−surface $PM_{2.5}$ relationship on annual or monthly time scales.[39] Evaluation of a global model ensemble using satellite AOD and aerosol vertical profile products over three key wildfire regions shows that most models underestimate AOD and the altitude of the wildfire aerosol layer during fire seasons, dominated by biomass burning aerosol errors.[40] So far there has been little success in converting AOD to surface $PM_{2.5}$ concentrations during wildfire events.

2. MATERIALS AND METHODS

2.1. Ground-Based Observations. We first use ground observations of AOD from the Aerosol Robotic Network (AERONET) at eight sites within the Alaska domain (Figure 1 and Table S1) to evaluate satellite and modelled AOD. The ground-based CIMEL sun/sky radiometer at each AERONET site provides AOD in nine spectral channels with low uncertainty (~0.01−0.02) and high temporal resolution under cloud-free conditions.[41] Here, we interpolate the AOD at 550 nm using the standard Ångström exponent (440−675 nm)[42] to match with the satellite AOD band. In this work we use version 3, level 2.0 AERONET AOD during summertime (May 1−August 31) from 2005 to 2019.

We include two sets of surface $PM_{2.5}$ measurements to evaluate modelled $PM_{2.5}$, as shown in Figure 1. The first data set is hourly $PM_{2.5}$ mass concentrations recorded since 2005 at five AirNow sites in Alaska (Table S2), measured using a beta attenuation monitor (BAM). The second data set comprises hourly surface $PM_{2.5}$ ambient concentrations collected since the summer of 2019 by the PurpleAir low-cost sensor network, which included 41 PurpleAir sensors across the state of Alaska in 2019 (Figure 1) and expanded to 106 sensors in 2022. The

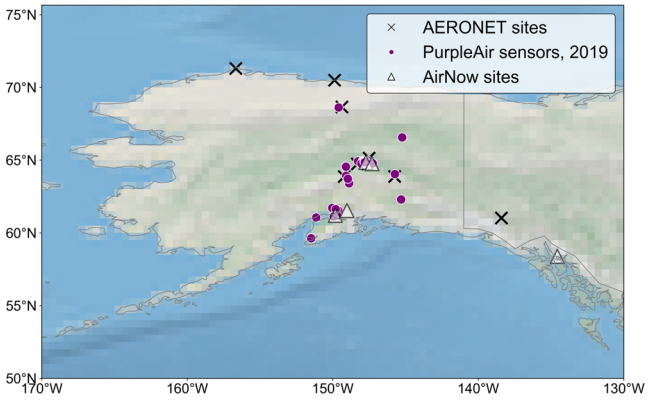

Figure 1. Locations of ground AOD and $PM_{2.5}$ measurements in Alaska. Black crosses are AERONET sites. Purple filled circles show PurpleAir sensors deployed in Alaska in the 2019 summer. White triangles are AirNow sites.

PurpleAir data use a conversion factor (CF) = 1, indicating "average particle density" for standard environment (indoors/chamber), with bias and correction discussed in section 3.1. For comparative analysis, we averaged the hourly $PM_{2.5}$ data from both AirNow and PurpleAir on a 24 h average daily basis.

2.2. Satellite Aerosol Retrievals. In this study, we use daily averaged high resolution gridded (0.1° × 0.1°) level 3 AOD at 550 nm from MODIS-Aqua and VIIRS-SNPP during the 2005−2019 and 2012−2019 summers over Alaska, respectively.[43−46] The quality control of level 3 products refers to Gupta et al.[46] The MODIS instruments aboard NASA Terra and Aqua satellites have been operating since 1999 and 2002, respectively. MODIS AOD retrievals have been widely used to characterize global and regional air quality distributions[47,48] and evaluate population exposure to PM.[33,49] The VIIRS instrument, on board NASA−NOAA SNPP and NOAA-20 satellites that were launched in 2011 and 2017, was designed as a new generation of satellite sensors that can extend and improve the aerosol products initiated by its predecessors. VIIRS aerosol algorithms, including Deep Blue (DB) and Dark Target (DT), inherit from the precedents established from MODIS.[17,50] The MODIS-Aqua and VIIRS-SNPP level 3 products both are created by fusing DT[51] and DB algorithm[52] retrieved level 2 AOD at 10 × 10 km^2 spatial resolution, ensuring the consistency of AOD from the two satellites in this study.[46]

Recent evaluation of MODIS AOD over AERONET sites in Alaska indicates the capability of MODIS AOD product in quantifying the air quality in Alaska during the summertime.[53] A global validation of VIIRS retrieved 550 nm AOD against AERONET shows a global uncertainty of ±(0.05 + 20%) (R = 0.82, mean bias = 0.01, root mean square error (RMSE) = 0.12), which is comparable to MODIS aerosol products; the VIIRS uncertainty at boreal regions (R = 0.82, mean bias = 0.01, RMSE = 0.16) aligns with the global values.[54] Following the recommendation from the Multi-sensor Aerosol Products Sampling System (MAPSS),[55] we use a 27.5 km radius circle buffer to extract spatially averaged AOD time series around AERONET AOD locations from MODIS-Aqua and VIIRS-SNPP.

We further use the data from the Cloud-Aerosol LIdar with Orthogonal Polarization (CALIOP) instrument on board the Cloud-Aerosol Lidar and Infrared Pathfinder Satellite Observation (CALIPSO).[56] CALIOP observes the backscattered radiations of simultaneous, co-aligned laser pulses it sends at

https://doi.org/10.1021/acsestair.4c00120
ACS EST Air 2024, 1, 1164−1176

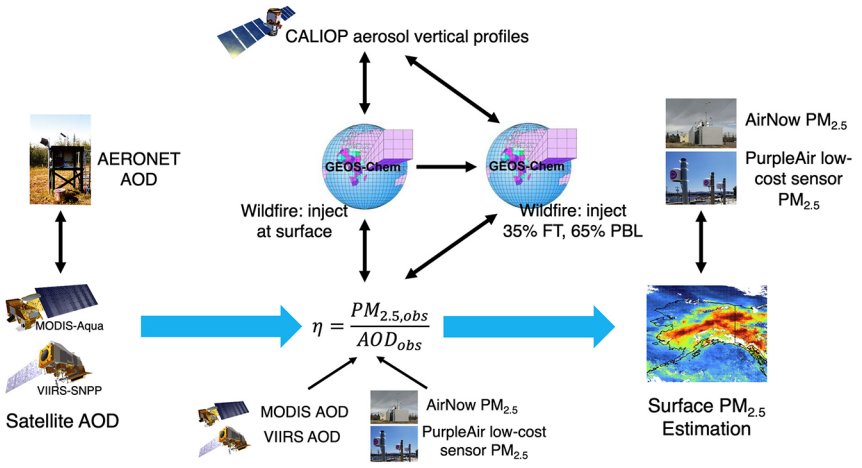

Figure 2. Workflow of evaluating AOD and $PM_{2.5}$ from satellite, model, and ground-based measurements and estimating surface $PM_{2.5}$ in Alaskan summer.

1064 and 532 nm. In this study, we use the CALIOP level 3 daytime cloud-free aerosol extinction vertical profiles version 4, for aerosol species together (Variable name: Extinction_Coefficient_532_Mean). The primary data sets in the CALIOP level 3 product are monthly mean AOD at 532 nm and vertical profiles of the aerosol extinction coefficient. This product is reported at 2° latitude × 5° longitude horizontal resolution and 60 m vertical resolution grid cells, based on quality screened CALIOP level 2 aerosol profiles and layer classification information.[57] CALIOP level 3 532 nm AOD is computed by first averaging the set of quality-screened aerosol extinction profiles for the month and then vertically integrating the mean extinction profile. CALIOP level 3 products are reported for all aerosol species together and for three individual aerosol species: dust, polluted dust, and smoke, since 2006. During the Alaskan wildfire seasons from 2006 to 2019, the predominant aerosol source was elevated smokes (Figure S1).

CALIOP level 3 aerosol product contains sampling biases, which could be mitigated through averaging and quality screening. CALIOP operates on a 16 day repeat cycle, and this temporal limitation could introduce sampling biases during comparisons to polar orbit satellite retrievals or daily ground-based observations. The coarse horizontal resolution of CALIOP level 3 product could smooth wildfire signals, resulting in a low bias in the monthly mean AOD and aerosol extinction profiles. Additionally, CALIOP may lose sensitivity to aerosols at lower altitudes or under low AOD conditions. In the meantime, these sampling biases can be reduced by the large data volume over a long study period (2006−2019), monthly averaging, and quality screening of the level 2 product. The quality screening reduces errors in layer detection, layer classification, extinction retrieval, and biases from surface signal anomalies. The "average-then-integrate" method for computing AOD could reduce potential low bias due to uneven sampling of the atmospheric geometric depths in different integrated profiles. Under consistent sampling conditions, CALIOP AOD shows a reasonable linear agreement with regridded MODIS data, though with a low bias (Figure 3g).

CALIOP AOD shows a low bias compared to AERONET and MODIS over land in northern high latitudes,[58] which could be due to the coarse spatial resolution, different wavelength, and possible missing AOD especially under extreme high and low aerosol loads, and due to quality screening. Quality filtering is relatively more aggressive over regions and can reduce AOD by 30% where aerosol loading is low, because the relatively fewer aerosol samples in the low AOD region could be more effectively impacted by rejecting even a small number of samples.[57] The low bias is reduced in CALIOP version 4 product compared to version 3, but differences between CALIOP and MODIS/VIIRS AOD are expected especially where the aerosol load is below CALIOP's detection limits.[58]

2.3. GEOS-Chem Simulations. We use a nested GEOS-Chem model (version 12.7.2, https://doi.org/10.5281/zenodo.3701669) to reproduce the regional 3-D distribution of aerosol mass and AOD. Two GEOS-Chem simulations are performed:

(a) In the control run, the wildfire emissions are injected at the surface layer. This configuration has been used in our previous work.[13,59]

(b) In the sensitivity run, 35% of wildfire emissions are injected to the free troposphere; 65% are injected within the planetary boundary layer (PBL). Other configurations are the same as in the control run.

Our nested simulations are performed over the Alaska domain ([50, 75]° N, [−170, −130]° E) during the summers (May 1−August 31) of 2005−2019. Driven by the assimilated meteorology from the Modern-Era Retrospective analysis for Research and Applications, version 2 (MERRA-2) by the Global Modeling and Assimilation Office (GMAO) at NASA's Goddard Space Flight Center (GSFC),[60] the nested simulation has a 0.5° × 0.625° horizontal resolution with 47 vertical layers and a transport time step of 15 min. The boundary conditions of the nested model are updated every 3 h from a global GEOS-Chem simulation at 2° × 2.5° resolution.

In this work, we use the detailed O_3−NO_x−HO_x−VOC chemistry ("tropchem" mechanism)[61−63] with online aerosol simulation including sulfate−nitrate−ammonium, primary and secondary organic aerosols (POA and SOA), black carbon (BC), sea salt, and dust. The sulfate−nitrate−ammonium−water system is modelled by the ISORROPIA II thermodynamic equilibrium model. The scheme of planetary boundary layer mixing follows a nonlocal scheme implemented by Lin and McElroy.[64] Biogenic VOC emissions are from MEGAN2.1.[65−67] Anthropogenic emissions are from the Community Emission Data System (CEDS).[68,69] Biomass burning emissions use the Global Fire Emission Database (GFED4.1s) biomass burning emissions processed for GEOS-Chem.[70] We use 3 h emissions

https://doi.org/10.1021/acsestair.4c00120
ACS EST Air 2024, 1, 1164−1176

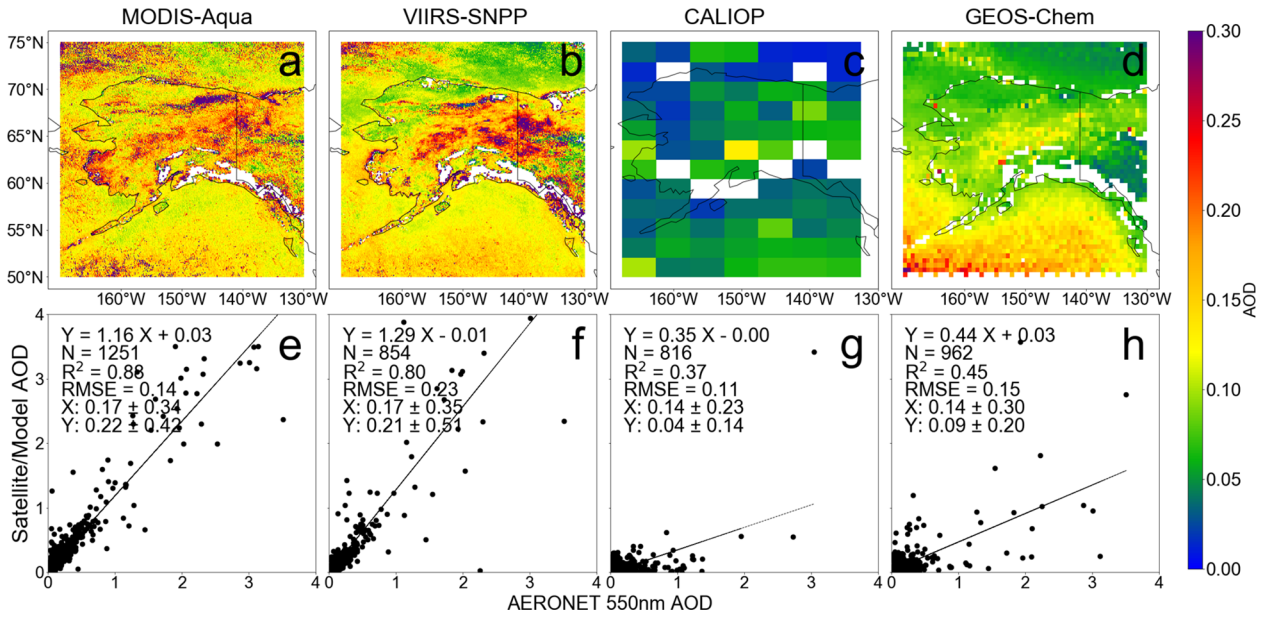

Figure 3. Comparison of AOD from AERONET, MODIS-Aqua, VIIRS-SNPP, CALIOP, and GEOS-Chem. (a–d) Spatial pattern of monthly mean AOD from MODIS-Aqua, VIIRS-SNPP, CALIOP, and GEOS-Chem in Alaska, averaged by daily data (except CALIOP) for 2006–2019 summers (2012–2019 summers for VIIRS-SNPP). (e, f, h) Scatterplots of daily AOD from MODIS-Aqua, VIIRS-SNPP, and GEOS-Chem (*Y*-axis) versus AERONET daily AOD (*X*-axis) at eight AERONET sites. (e, h) Summers of 2006–2019; (f) summers of 2012–2019. (g) Scatterplots of monthly 532 nm AOD from CALIOP versus monthly 550 nm AOD from regridded MODIS-Aqua, in 2006–2019 summers. In each panel of (e)–(h), texts show the linear regression parameters, number of points, R^2, RMSE, and the mean and standard deviation values of *X* and *Y*.

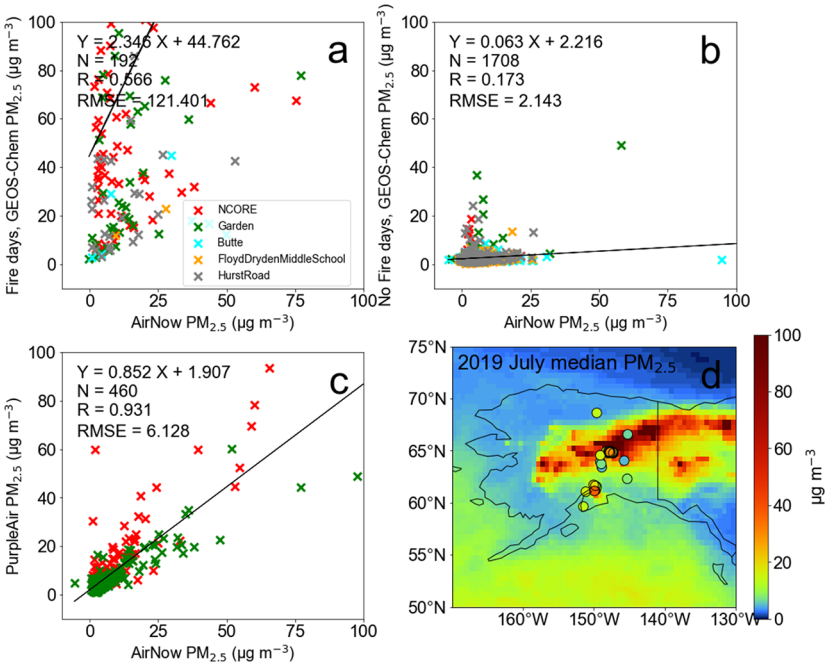

Figure 4. Scatterplot of daily surface $PM_{2.5}$ at AirNow and PurpleAir sites. (a) GEOS-Chem versus AirNow daily surface $PM_{2.5}$, during fire days (AOD > 0.5) from May to August in 2005–2019. Red, green, cyan, orange, and gray crosses are daily data pairs at NCore, Garden, Butte, Floyd Dryden Middle School, and Hurst Road sites. (b) Similar to (a) but in nonfire days (AOD < 0.1). (c) PurpleAir versus AirNow daily surface $PM_{2.5}$, from May to August in 2019. PurpleAir data are corrected based on eq 1. (d) GEOS-Chem monthly median surface $PM_{2.5}$ in Alaska, July 2019. Dots show monthly median $PM_{2.5}$ from 41 PurpleAir sensors in July 2019.

calculated in GFED4.1s based on fire detection and burning area from the MODIS satellite.[71]

2.4. Workflow. Figure 2 shows the workflow of this study. The workflow contains five parts: (a) evaluation of AOD from MODIS-Aqua, VIIRS-SNPP, CALIOP, and GEOS-Chem using eight AERONET sites in Alaska, for the summers of 2005–2019; (b) evaluation of surface $PM_{2.5}$ from PurpleAir sensors and GEOS-Chem using surface $PM_{2.5}$ measurements from five AirNow sites in Alaska, for the summers of 2005–2019; (c) comparison between modelled and observational AOD–$PM_{2.5}$ relationships under various AOD ranges and comparison between modelled and observational proportions of AOD

https://doi.org/10.1021/acsestair.4c00120
ACS EST Air 2024, 1, 1164–1176

within the PBL, under various AOD ranges; (d) performance of the GEOS-Chem sensitivity run to evaluate the impact of increasing wildfire injection height on aerosol vertical distribution and the AOD−$PM_{2.5}$ relationship; (e) estimation of surface $PM_{2.5}$ over Alaska by applying the observational AOD−$PM_{2.5}$ relationship to satellite AOD, for the 2021 and 2022 Alaskan summers. PurpleAir $PM_{2.5}$ in these two years is used to evaluate the satellite derived $PM_{2.5}$.

3. RESULTS

3.1. Evaluation of AOD and Surface-Level $PM_{2.5}$ in Alaskan Summertime. Figure 3 compares the monthly AOD products from MODIS-Aqua, VIIRS-SNPP, CALIOP, and GEOS-Chem in the Alaskan summers of 2006−2019. To calculate the monthly patterns, VIIRS-SNPP, CALIOP, and GEOS-Chem AOD are resampled based on the data availability of MODIS-Aqua AOD, which was initially regridded to match the corresponding horizontal resolution. We show in Figure 3e,f that MODIS-Aqua and VIIRS-SNPP AOD are in excellent agreement with AERONET AOD from eight sites in Alaska for the summers of 2005−2019, with biases less than 30%. The good linear agreement between satellite and AERONET AOD is exhibited across the entire AOD range in Alaska, which spans approximately 0−3, indicating a relatively minor issue with AOD saturation in satellite measurements during Alaskan fire periods. The two satellite AOD show similar temporal and spatial variabilities (Figure 3a,b,e,f), with enhanced AOD over interior Alaska where most boreal forest fires occur. In Figure 3c, despite its much coarser resolution, CALIOP AOD also shows enhancements over interior Alaska similar to those observed in MODIS-Aqua and VIIRS-SNPP AOD. This highlights the potential of using CALIOP to evaluate Alaskan summertime aerosol vertical profiles on a monthly scale. The low bias of CALIOP AOD relative to MODIS-Aqua and VIIRS-SNPP can be in part due to diluted wildfire signal during the spatiotemporal average in a relatively coarse resolution and in part due to the large attenuation by heavy smoke that affects the retrieval of total column. This low bias is consistent with previous global AERONET evaluation against CALIOP version 4 total column AOD in Alaska.[58]

We further compare GEOS-Chem with the three satellite AOD products and the AERONET AOD. We show in Figure 3d that GEOS-Chem AOD is lower than that of MODIS-Aqua and VIIRS-SNPP but still captures the AOD enhancements over interior Alaska largely due to wildfires. Overall, the GEOS-Chem AOD is around 44% of the AERONET AOD (Figure 3h), but the correlation with AERONET is diminished compared to the satellite products, likely due to inaccuracies in the model's representation of wildfire emissions. The discrepancy between modelled and satellite AOD over the Gulf of Alaska may be attributed to issues in the model's representation of sea salt aerosols.[72]

Figure 4 illustrates the evaluation of 24 h mean daily surface $PM_{2.5}$ from GEOS-Chem and the PurpleAir network, using AirNow $PM_{2.5}$ measurements from five sites in Alaska during the summers of 2005−2019. The surface $PM_{2.5}$ enhancement in Alaskan summertime is primarily attributed to wildfires. Here we classify days with AOD > 0.5 and AOD < 0.1 as fire and nonfire days, respectively. Figure 4a,b shows that, during nonfire days, GEOS-Chem surface $PM_{2.5}$ is underestimated compared to AirNow measurements ($Y = 0.03X + 2.28$), while in fire days GEOS-Chem overestimates surface $PM_{2.5}$ by a factor of 2.36, especially over NCore and Garden sites where there are significant wildfire activities. The model demonstrates limited skills in accurately representing the variability of $PM_{2.5}$ compared to AirNow measurements both during fire days ($R = 0.57$) and nonfire days ($R = 0.09$). This limitation is likely attributed to the challenges in estimating wildfire emissions, simulating the aerosol physical and chemical processes, as well as the spatial and temporal evolution of wildfire plumes.

The raw PurpleAir $PM_{2.5}$ correlates well with AirNow $PM_{2.5}$ in the 2019 Alaskan summer but is a factor of 1.72 higher than the latter. Several studies have examined the possible bias and correction for PurpleAir $PM_{2.5}$.[73−77] In particular, Barkjohn et al.[76] developed a U.S.-wide correction for PurpleAir $PM_{2.5}$:

$$\text{corrected PurpleAir } PM_{2.5} = \text{raw PurpleAir } PM_{2.5}(\text{CF} = 1) \times 0.524 - \text{RH} \times 0.0862 + 5.75 \quad (1)$$

In eq 1, raw PurpleAir $PM_{2.5}$ is the average of channels A and B from the higher correction factor (CF = 1) and RH is the relative humidity in percent.

We find that PurpleAir $PM_{2.5}$ corrections based on colocated AirNow measurements (Figure 4c) are in good agreement with the EPA U.S.-wide correction (Figure S2), exhibiting a bias of approximately 10% and an RMSE of around 3.08 $\mu g\ m^{-3}$, which is consistent with the previous study.[76] This suggests the efficacy of the EPA's U.S.-wide correction approach for PurpleAir $PM_{2.5}$ in Alaskan summers. In this work, we follow the EPA U.S.-wide correction method (eq 1) to correct all PurpleAir $PM_{2.5}$ in Alaska during summertime. Figure 4c shows that the corrected PurpleAir $PM_{2.5}$ has a good agreement with AirNow $PM_{2.5}$ at NCore and Garden sites ($Y = 0.85X + 1.91$, $R = 0.93$, RMSE = 6.13).

Figure 4d shows the monthly median surface $PM_{2.5}$ from both GEOS-Chem and available PurpleAir sensors for July 2019. GEOS-Chem and the PurpleAir network show good agreement in the spatial distribution of surface $PM_{2.5}$, largely driven by wildfires. We also show that surface $PM_{2.5}$ from GEOS-Chem tends to have a high bias compared to that from PurpleAir, especially over wildfire plumes.

3.2. Evaluation of AOD−$PM_{2.5}$ Relationship in Alaskan Summer. The AOD−$PM_{2.5}$ relationship is quantified by the conversion factor

$$\eta = \frac{\text{surface } PM_{2.5}}{\text{AOD}} \quad (2)$$

Here we calculate η by using the 24 h average surface $PM_{2.5}$ and the local noon average AOD. The 24 h average surface $PM_{2.5}$ and satellite AOD have been linked together in previous studies.[78−81] Ground-based measurements also demonstrate a good correlation ($Y = 0.86X + 2.61$, $R = 0.81$, RMSE = 16.27) between the local noon average and 24 h average surface $PM_{2.5}$ (Figure S9), supporting the practicality of linking the satellite daytime AOD with 24 h average $PM_{2.5}$.

To capture the short-term variability of wildfire smokes, while increasing data availability and the robustness of the statistics, we analyze the η−AOD relationship for GEOS-Chem and observations on a weekly basis. In this analysis, we adjust modelled AOD and $PM_{2.5}$, as well as satellite AOD, using the linear regression slope obtained from comparisons with standard measurements shown in Figures 3 and 4, to ensure a collocated comparison. For the summers of 2005−2019, we calculate the weekly η_{obs} using MODIS-Aqua/VIIRS-SNPP AOD and surface $PM_{2.5}$ from five AirNow sites and 41 PurpleAir sensors. Additionally, we compute weekly η_{GC} using 24 h averaged

https://doi.org/10.1021/acsestair.4c00120
ACS EST Air 2024, 1, 1164−1176

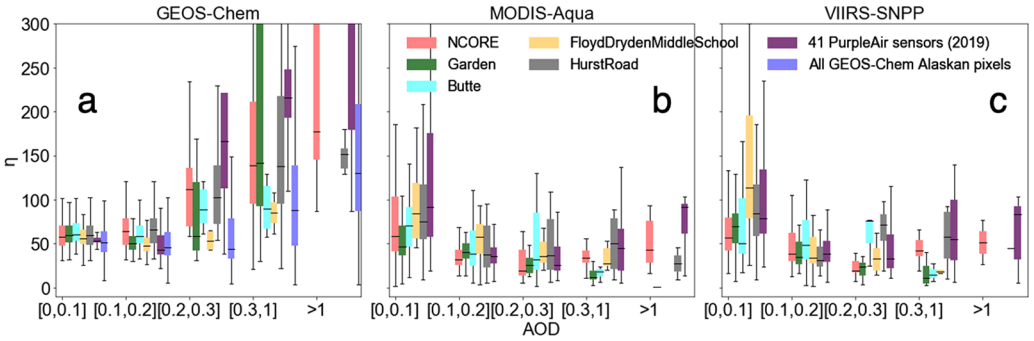

Figure 5. η−AOD relationship from model and observations in Alaskan summertime. (a) Boxplot of weekly η_{GC} from GEOS-Chem under various AOD ranges, in 2005−2019 summers. Red, green, cyan, orange, and gray boxes represent the statistics of weekly η within 27.5 km radius circle around NCore, Garden, Butte, Floyd Dryden Middle School, and Hurst Road sites. Purple and blue boxes represent weekly η statistics for 41 PurpleAir sites and for all GEOS-Chem continental pixels in Alaska. (b) Boxplot of weekly η_{obs} from MODIS-Aqua AOD and AirNow $PM_{2.5}$ surface measurements under different AOD ranges. (c) Similar to (b) but using VIIRS-SNPP AOD.

surface $PM_{2.5}$ and local noon averaged total column AOD, similar to a previous study.[32] Weekly η values are the ratio between the weekly mean $PM_{2.5}$ and weekly mean AOD. Both η_{obs} and η_{GC} are binned into five AOD ranges: [0, 0.1], [0.1, 0.2], [0.2, 0.3], [0.3, 1], and >1.

In Figure 5a, we show a sharp increase in η_{GC} as AOD rises, with the median value exceeding 100 when AOD > 1. Notably, the dependency of η_{GC} on AOD seems consistent across five AirNow sites and 41 PurpleAir sites. The high bias in η_{GC} at AOD > 0.3 is expected as the model tends to underestimate AOD and overestimate surface $PM_{2.5}$ (Figures 3 and 4).

η_{obs}, though exhibiting a high variability, presents a weak dependence on AOD and significantly lower values than η_{GC} when AOD > 1. Below an AOD threshold of 0.3, η_{obs} remains stable and slightly decreases, in line with η_{GC}; when AOD > 0.3, η_{obs} increases with a much weaker increasing rate (25−50%) than η_{GC} does, as shown in Figure 5b,c. The case study conducted at the NCore site during the 2005−2019 summertime period shows a stable magnitude of weekly η_{obs} (Figure S4), representing a weak dependence of η_{obs} on AOD which is consistent with the η_{obs}−AOD relationship in Figure 5b. η_{obs} could exhibit high variability in low and high AOD conditions. The high variability of η_{obs} under low AOD conditions (up to 300% when AOD < 0.1) does not significantly impact the estimated $PM_{2.5}$ level using eq 2, due to the low AOD levels. The high variability of η_{obs} under high AOD during strong wildfires could be attributed to the spatial heterogeneity of wildfire plumes, making it challenging to effectively estimate η_{obs} during wildfires.

Similar patterns of the η_{GC}−AOD and η_{obs}−AOD relationships are also shown in daily and monthly bases (Figure S8). The daily based η_{obs} values have more available data points compared to weekly and monthly based η_{obs}, but they can show larger variability due to the strong daily variability of wildfire smokes. Across daily, weekly, and monthly bases, the η_{GC}−AOD relationship shows a significant increasing trend when AOD > 0.3, while η_{obs} appears to have a weaker dependence on AOD. This discrepancy highlights a significant overestimation in η_{GC} under high AOD, which could be qualitatively confirmed despite both η_{GC} and η_{obs} exhibiting substantial variability within each AOD bin. The η_{GC}−η_{obs} discrepancy under high AOD could be due to systematic biases in the model during wildfires.

The variations of η_{obs} and η_{GC} during wildfire progresses are further examined through a case study conducted at the NCore site during the 2005−2019 summers (Figure S4). During periods of intense wildfire activities, especially three strong fire periods in the summers of 2009, 2015, and 2019, η_{GC} rises to >300 as the modelled wildfire $PM_{2.5}$ reaches a maximum. In contrast, η_{obs} shows a similar magnitude to η_{GC} during weak fire periods but does not show significant increases in the three strong fire periods. This is consistent with the η_{obs}−AOD and η_{GC}−AOD relationships shown in Figure 5. In GEOS-Chem, during strong wildfires, organic carbon accounts for the majority (~90%) of total AOD, while black carbon accounts for around 5% of total AOD; outside wildfire periods, organic carbon takes around 10−50% of total AOD while the proportion of black carbon is negligible (Figure S7).

In cases of exceptionally intense wildfires, it's possible that η could be affected by AOD saturation issues. The availability of data during periods of strong wildfires (AOD > 1) is relatively limited compared to conditions of weaker fire activity (AOD < 0.3), potentially introducing uncertainties into η_{obs} and η_{GC} values under high AOD in Figure 5. To thoroughly investigate the impact of AOD saturation issues on η_{obs}, a more extensive observational record of AOD and $PM_{2.5}$ levels in Alaska during intense wildfire events is essential.

3.3. Evaluation of Aerosol Vertical Profiles. To explore the influence of aerosol vertical profiles on the η_{obs}−η_{GC} discrepancy, we employ two independent approaches: (a) assessing the sensitivity of η_{GC} to the variations in the proportion of wildfire emissions within PBL; (b) evaluating aerosol vertical profiles using satellite lidar data.

Figure S6 shows that, at the NCore site during the summer of 2019, allocating 35% of the total wildfire emission into the free troposphere results in a 30% decrease in modelled $PM_{2.5}$ levels and η_{GC} under strong wildfires (daily surface $PM_{2.5}$ > 200 $\mu g\ m^{-3}$), thereby improving the consistency with η_{obs} and AirNow $PM_{2.5}$ measurements. However, the modelled $PM_{2.5}$ based on the adjusted injection height still exhibits an overestimation compared to AirNow measurements, by a factor of 1.6. Thus, further refinements are *warranted* to accurately correct the modelled $PM_{2.5}$ during fire days.

We utilize CALIOP level 3 aerosol extinction vertical profiles to characterize the aerosol vertical distributions across various AOD ranges and examine the model biases. We introduce f_{PBL} as a metric to quantify the fraction of AOD within the PBL relative to the total column of AOD. f_{PBL} is defined as

$$f_{PBL} = \frac{AOD_{PBL}}{AOD} \quad (3)$$

https://doi.org/10.1021/acsestair.4c00120
ACS EST Air 2024, 1, 1164−1176

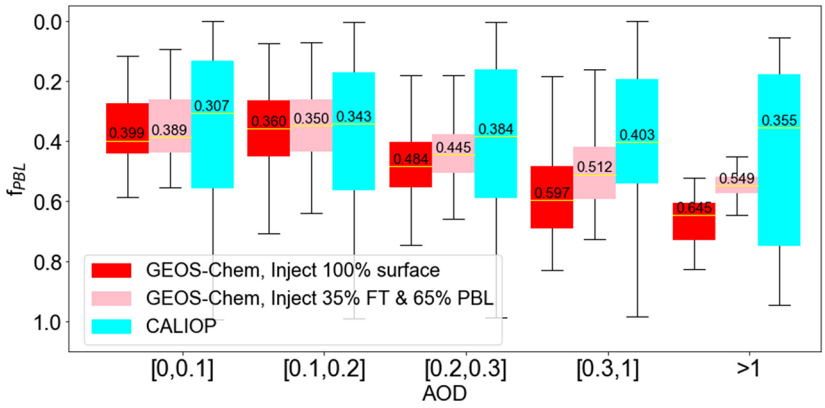

Figure 6. f_{PBL}–AOD relationship from model and observations in Alaskan summertime. f_{PBL} across different AOD ranges, from GEOS-Chem and CALIOP. The red, pink, and cyan boxes represent monthly f_{PBL} statistics from GEOS-Chem with wildfire emissions injected at the surface, GEOS-Chem with 35% of wildfire emissions injected into the free troposphere and 65% within the PBL, and CALIOP, respectively, across specific AOD ranges over the Alaska domain during the summers from 2006 to 2019.

Here AOD_{PBL} represents the aerosol optical depth integrated from surface to the top of the PBL. We calculate f_{PBL} across all Alaskan continental pixels using GEOS-Chem and CALIOP monthly extinction coefficients in the 2006–2019 summertime period. The PBL height (PBLH) is obtained from the MERRA-2 data set. Figure 3c,g shows that CALIOP AOD, despite exhibiting a low bias compared to VIIRS-SNPP and AERONET AOD, is able to capture the AOD enhancement over interior Alaska and the Gulf of Alaska. A case study at the NCore site (Figure S5) shows that, during wildfire periods in interior Alaska, both GEOS-Chem and CALIOP present AOD and AOD_{PBL} enhancements. In the meantime, Figure S3 shows a linear relationship between CALIOP f_{PBL} and η_{obs} at the NCore site during the 2006–2019 summers, indicating the capability of CALIOP to capture the proportion of aerosol loading within the PBL during strong wildfire events on a monthly basis. Previous studies also show that CALIOP aerosol products exhibit sensitivity in detecting aerosol plumes within the PBL in the presence of wildfire smokes.[82,83] Despite the limited global coverage provided by CALIOP, we assert that this long-term record (2006–2019) offers sufficient statistical power to be representative of the Alaskan summer wildfire season.

Figure 6 shows that observational f_{PBL} remains low under all AOD ranges while GEOS-Chem suggests high f_{PBL} under high AOD. When AOD < 0.3, f_{PBL} from both GEOS-Chem and CALIOP are very similar to a median value around 0.39–0.47. When AOD > 0.3, f_{PBL} from CALIOP remains low (0.36), while the GEOS-Chem f_{PBL} rises to 0.64 when AOD > 1. The persistent low f_{PBL} in CALIOP when AOD > 0.3 is consistent with the weak dependence of η_{obs} on AOD (Figure 5), as they both suggest that the fraction of near surface aerosol loading to the total column does not increase significantly with increasing AOD. In contrast, we show the model deviates from observations in both f_{PBL} and η under high AOD conditions. Modelled η_{GC} and observational η_{obs} both increase with f_{PBL} rising, but η_{GC} increases faster than η_{obs} under high f_{PBL}, indicating that the overestimation of f_{PBL} and η_{GC} in the model is consistent (Figure S3).

Figure 6 also shows that increasing wildfire emission injection height could reduce modelled f_{PBL} by 15% when AOD > 0.3, leading to a better agreement with the CALIOP observations. This is consistent with previous studies that suggest increasing plume injection height with strong wildfire plumes.[84−86] In Figure 6, increasing injection height only leads to a minor influence (<15%) on modelled f_{PBL}, and large discrepancy still exists between the adjusted modelled f_{PBL} and that from CALIOP. This indicates that an underestimated injection height of wildfire emissions in GEOS-Chem could partly explain the overestimated surface $PM_{2.5}$ and η_{GC}, but model overestimation in f_{PBL} and η_{GC} may be difficult to correct by adjusting the fraction of wildfire injection between the free troposphere and the PBL.

The analysis of the f_{PBL}–AOD relationship is not directly used to derive η'_{obs}, but it provides independent qualitative insights into the aerosol vertical distribution across different AOD levels. These results can corroborate the η_{obs}–AOD relationship.

3.4. Estimating Surface $PM_{2.5}$ Using Observational η_{obs}–AOD Relationship. In this section, we estimate surface $PM_{2.5}$ using the η_{obs}–AOD relationship and compare the estimates with PurpleAir ground-based measurements.

Figure 5b,c presents similar median values of η_{obs}, derived from observations across various locations in Alaska. Figure S4 demonstrates that the η_{obs}–AOD relationship remains consistent across different summers from 2006 to 2019 in Alaska. This consistency suggests that η_{obs} within specific AOD ranges, particularly under high AOD conditions, tends to be largely homogeneous across the Alaskan domain and exhibits stability over different years. To provide an observation-based estimation method of surface $PM_{2.5}$ over the Alaska domain, we assume that η_{obs} is a piecewise function across varying AOD ranges and does not change with time. We construct the piecewise function for η_{obs} based on VIIRS-SNPP AOD and PurpleAir $PM_{2.5}$ over Alaska in the 2019 summer:

$$\eta'_{obs} = \begin{cases} 79.07, & 0 < AOD \le 0.1 \\ 38.66, & 0.1 < AOD \le 0.2 \\ 32.76, & 0.2 < AOD \le 0.3 \\ 54.62, & 0.3 < AOD \le 1 \\ 83.96, & AOD > 1 \end{cases} \quad (4)$$

In eq 4, the value of η'_{obs} for each AOD range is the median value of weekly η_{obs} derived from VIIRS-SNPP AOD and PurpleAir $PM_{2.5}$ at 41 PurpleAir sensors during the summer of 2019 (Figure 5c). By inputting daily VIIRS-SNPP AOD to eq 4, we can obtain η'_{obs} over the whole Alaska on a daily basis.

https://doi.org/10.1021/acsestair.4c00120
ACS EST Air 2024, 1, 1164−1176

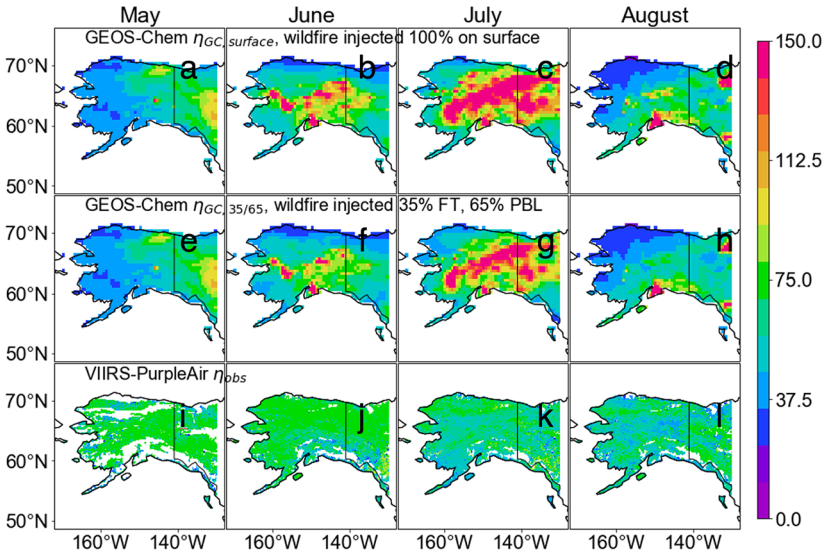

Figure 7. Modelled and observational monthly η in 2019 Alaskan summer. (a–d) Monthly $\eta_{GC,surface}$ averaged from weekly $\eta_{GC,surface}$, based on GEOS-Chem simulation that injects wildfire emissions at surface layer. (e–h) Monthly $\eta_{GC,35/65}$, based on GEOS-Chem simulation that injects 35 and 65% of wildfire emissions in the free troposphere and within the PBL. (i–l) Monthly η'_{obs} averaged from daily η'_{obs}, which is calculated based on eq 4 and VIIRS-SNPP daily AOD.

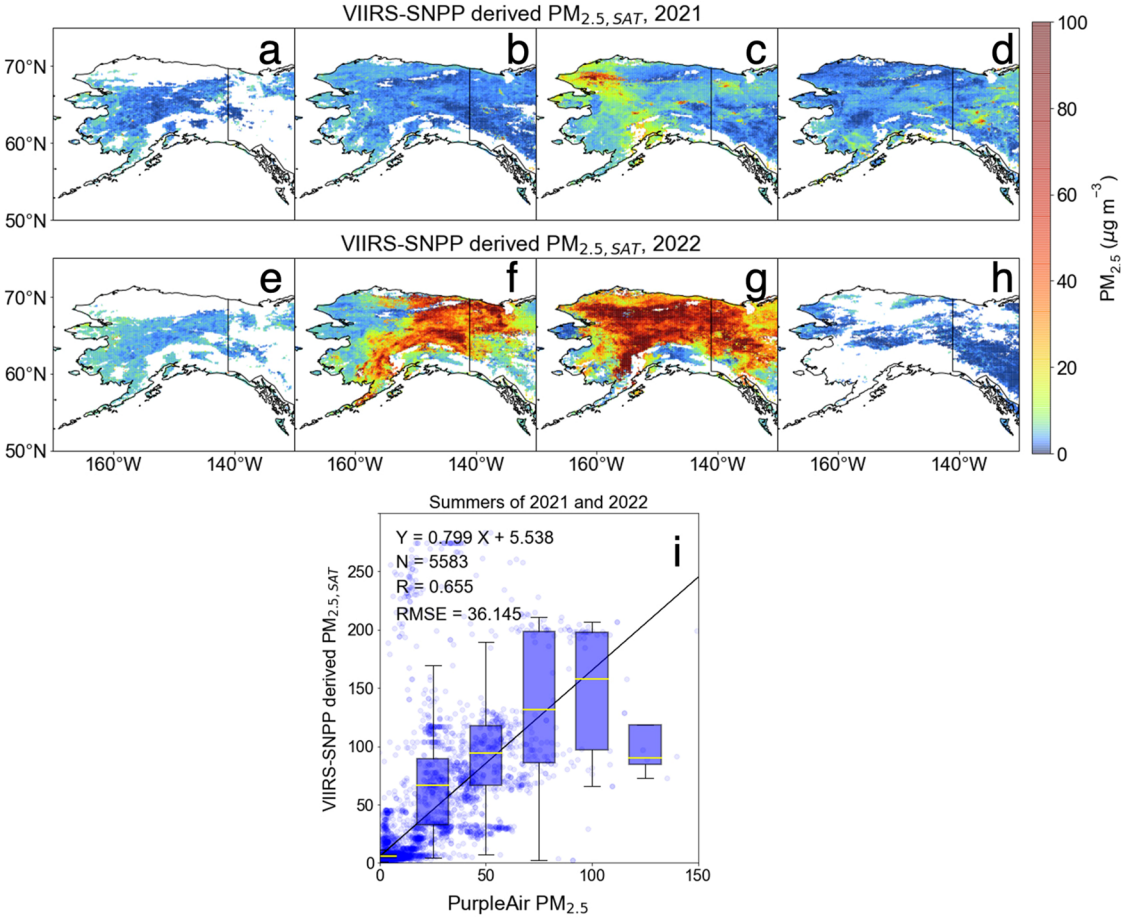

Figure 8. Satellite AOD derived surface $PM_{2.5,SAT}$ based on daily η'_{obs} calculated by eq 4 from VIIRS-SNPP daily AOD. (a–d) Monthly mean surface $PM_{2.5,SAT}$ derived from VIIRS-SNPP AOD, in Alaska in 2021 summer. (e–h) Similar to (a)–(d) but in 2022 summer. (i) Scatterplot of VIIRS-SNPP derived $PM_{2.5,SAT}$ versus PurpleAir $PM_{2.5}$ in Alaska in 2021 and 2022 summers. Blue boxes are boxplot of satellite derived $PM_{2.5,SAT}$ in each PurpleAir $PM_{2.5}$ bin. Yellow bars are median values of each box.

Additionally, we calculate the spatiotemporal patterns of weekly $\eta_{GC,surface}$ and $\eta_{GC,35/65}$ from the GEOS-Chem control run and sensitivity run. $\eta_{GC,surface}$ is derived from the GEOS-Chem control run, which assumes 100% of wildfire emissions are

https://doi.org/10.1021/acsestair.4c00120
ACS EST Air 2024, 1, 1164–1176

injected at the surface. In contrast, $\eta_{GC,35/65}$ is derived from a GEOS-Chem sensitivity run where 35% of wildfire emissions are injected into the free troposphere and 65% into the PBL.

Figure 7 illustrates the monthly patterns of $\eta_{GC,surface}$, $\eta_{GC,35/65}$, and η'_{obs} over Alaska during the summer of 2019. Figure 7a–d shows that the hotspots of $\eta_{GC,surface}$ (the pixels with η_{GC} >150 $\mu g\ m^{-3}$) are primarily located in interior Alaska, with locations shifting throughout the month due to wildfire development. Increasing wildfire injection height reduces the magnitude of $\eta_{GC,35/65}$ by around 30% over hotspots, in better agreement with η_{obs}. Although improved, $\eta_{GC,35/65}$ is still overestimated (Figure 7e–h), as indicated by the high biased $PM_{2.5}$ in the sensitivity test (Figure S6) which is a factor of 1.6 higher than AirNow $PM_{2.5}$ measurements in the 2019 summer. Compared to $\eta_{GC,35/65}$, η'_{obs} is more homogeneous and has a lower magnitude (Figure 7i–l). The closer agreement between η'_{obs} *and* $\eta_{GC,35/65}$ suggests that underestimating wildfire emission injection height may contribute to the model–observation discrepancy in η. Figure S4c shows that surface $PM_{2.5}$ estimated by using weekly η_{obs} could reproduce the daily variability of surface $PM_{2.5}$ measurements during wildfires. η'_{obs} is particularly valuable as it offers a straightforward method to estimate surface $PM_{2.5}$ across Alaska using satellite AOD, which is practical for future air quality monitoring operations.

We calculate daily surface $PM_{2.5}$ concentrations over the Alaskan summertime, using the piecewise function η'_{obs} from eq 4 and satellite daily AOD:

$$PM_{2.5,SAT} = \eta'_{obs} AOD \quad (5)$$

The η'_{obs} piecewise function is derived from observations in the summer of 2019 and is used to estimate surface $PM_{2.5}$ for the Alaskan summers of 2021 and 2022. This approach avoids a circular problem and evaluates the capability of the piecewise function in reproducing the magnitude and spatial variation of surface $PM_{2.5}$ over Alaska during summertime. The primary goal of η'_{obs} is to estimate $PM_{2.5}$ levels under different aerosol loadings, with the daily variability of estimated $PM_{2.5,SAT}$ mainly driven by the daily variability in satellite AOD.

Figure 8a–d and e–h show the estimated monthly mean surface $PM_{2.5,SAT}$ derived from VIIRS-SNPP AOD using η'_{obs} from eq 4, in the summers of 2021 and 2022, respectively. In the 2022 summer, satellite derived $PM_{2.5,SAT}$ shows an enhancement over interior Alaska, although the spatial pattern differs from that of 2019 (Figure S10) due to varying spatiotemporal patterns of wildfire smokes between the two years. In contrast, the summer of 2021 shows much lower $PM_{2.5,SAT}$ enhancements compared to 2019 and 2022, reflecting the lower wildfire activity in 2021.

We then compare $PM_{2.5,SAT}$ to colocated PurpleAir $PM_{2.5}$ measurements for the summers of 2021 and 2022. As shown in Figure 8i, $PM_{2.5,SAT}$ has a good agreement with 64 and 106 PurpleAir sensors in 2021 and 2022 ($Y = 0.80X + 4.7$, $R = 0.66$), though η'_{obs} is calculated based on 2019 data when the PurpleAir network had less spatial coverage. This indicates that η'_{obs} can effectively estimate $PM_{2.5}$ in locations where ground measurements were not available in 2019. In Figure 8a–h, $PM_{2.5,SAT}$ suggests elevated surface $PM_{2.5}$ levels in Yukon Flat and tribal villages, underscoring the need for increased $PM_{2.5}$ monitoring in these regions *inhabited by underrepresented groups*. Our method demonstrates the potential for filling gaps in $PM_{2.5}$ estimation where surface measurements are limited. In addition, our model sensitivity test for the summer of 2019 suggests that increasing the wildfire emission injection height can improve modelled $PM_{2.5}$. However, further adjustments are needed to reduce the overestimation in $\eta_{GC,36/65}$ and the modelled $PM_{2.5}$.

4. DISCUSSION

In this work, we present a piecewise function η'_{obs} across various AOD ranges, utilizing it to compute the 24 h average daily surface $PM_{2.5}$ from satellite AOD (eq 4, Figures 7 and 8). The η'_{obs} piecewise function is established based on the η_{obs}–AOD relationship derived from ground $PM_{2.5}$ measurements and satellite AOD. The η_{obs}–AOD relationship indicates a lower proportion of aerosols at the near surface layer, which can be corroborated with CALIOP aerosol vertical profile retrievals and GEOS-Chem sensitivity simulations that involve raising the wildfire emission injection height. During wildfire periods, η_{obs} can exhibit large variabilities within an AOD bin, yet it effectively captures the overestimation in modelled η_{GC}. This indicates that our piecewise function η'_{obs} is capable of estimating $PM_{2.5}$ with reasonable accuracy. The satellite derived surface $PM_{2.5,SAT}$, estimated by the η_{obs}–AOD relationship from the 2019 Alaskan summer, shows a reasonable agreement with PurpleAir measurements for 2021 and 2022 Alaskan summers. This highlights the efficacy of our approach in estimating surface $PM_{2.5}$ in Alaska, particularly in remote regions that are affected by intense wildfire smoke and lacking ground measurements.

Our study underscores several significant challenges in estimating surface $PM_{2.5}$ during Alaskan summer wildfire seasons. We show that the model representation of aerosol vertical profiles over a wildfire region is often ill-posed, resulting from the wildfire injection scheme and vertical mixing. This is further supported by the GEOS-Chem sensitivity test with increasing wildfire injection height, as well as CALIOP satellite retrieval (Figure 6). Injecting 35% of total wildfire emissions to the free troposphere could lead to a 30% reduction in surface $PM_{2.5}$ and η_{GC}, along with a 15% decrease in f_{PBL} during strong wildfire events. Despite these improvements, the modelled $PM_{2.5}$ remains overestimated by a factor of 1.6, indicating the need for further improvements in the model before an accurate η_{GC} and surface $PM_{2.5}$ simulation can be achieved.

Despite the improvement in deriving surface $PM_{2.5}$ from AOD, we emphasize that this observational η'_{obs} warrants further investigation.

First, η_{obs} exhibits significant variability within specific AOD bins, particularly when AOD > 0.3. This variability could potentially impact the effectiveness of η'_{obs} in representing the AOD–$PM_{2.5}$ relationship during intense wildfires. The high variability of η_{obs} could be due to the following: (a) The coarse AOD bins may blend multiple wildfire events with different aerosol vertical distributions into one AOD bin, leading to mixed signals in η_{obs} in each AOD bin. (b) The statistical robustness of η_{obs} is limited by the availability of observation data. (c) The piecewise function approach may oversimplify the spatiotemporal variability of η and its dependence on other variables, introducing biases in the estimation process.

Second, the observational relationship does not take into account the scenarios when plumes are largely aloft. In this case, satellite AOD is high but surface $PM_{2.5}$ levels remain low. This scenario is likely less an issue for daily $PM_{2.5}$ than for hourly $PM_{2.5}$.

Third, we show that satellite derived $PM_{2.5}$ can be too low when surface $PM_{2.5}$ is higher than 200 $\mu g\ m^{-3}$, suggesting further improvement is needed under extremely smoky conditions. The piecewise function can be further improved by increasing AOD

https://doi.org/10.1021/acsestair.4c00120
ACS EST Air 2024, 1, 1164–1176

bins and accounting for more variables, with more ground-based measurements including low-cost sensors becoming available.

■ ASSOCIATED CONTENT

Data Availability Statement

The code used to process the data and plot figures is available on github: https://zenodo.org/account/settings/github/repository/Holton1/Codes-for-Observational-constraints-on-AOD-PM2.5-relationship-during-Alaskan-wildfire-seasons. The data we used in this study is available on figshare: https://figshare.com/articles/dataset/Data_for_the_paper_Observational_constraints_on_AOD-surface_PM2_5_relationship_during_Alaskan_wildfire_seasons_submitted_to_ACS_ES_T_Air_Manuscript_ID_ea-2023-00093n_/25909300.

Supporting Information

The Supporting Information is available free of charge at https://pubs.acs.org/doi/10.1021/acsestair.4c00120.

Details of eight AERONET and five AirNow sites in Alaska; monthly mean partial AOD from specific aerosol type in CALIOP level 3 data; scatterplot comparing PurpleAir $PM_{2.5}$ corrected by simple linear slope versus PurpleAir $PM_{2.5}$ corrected by U.S.-wide correction from ref 76; scatterplot of η under different f_{PBL} ranges, from model and observation; time series plot of daily η and $PM_{2.5}$ from model and observation; time series plot of monthly AOD for total column and within PBL, from model and observation; time series plot of daily η and $PM_{2.5}$ from model, applying different wildfire injection heights; time series of proportion of black carbon and organic carbon in total column AOD; η−AOD relationships from model and observation, in daily and monthly bases; scatterplot of AirNow daily $PM_{2.5}$, local noon average versus 24 h average (PDF)

■ AUTHOR INFORMATION

Corresponding Authors

Tianlang Zhao − *Geophysical Institute and Department of Chemistry and Biochemistry, University of Alaska Fairbanks, Fairbanks, Alaska 99775, United States;* orcid.org/0009-0009-9480-1389; Phone: 907-750-9986; Email: tzhao@alaska.edu

Jingqiu Mao − *Geophysical Institute and Department of Chemistry and Biochemistry, University of Alaska Fairbanks, Fairbanks, Alaska 99775, United States;* orcid.org/0000-0002-4774-9751; Phone: 907-474-7118; Email: jmao2@alaska.edu

Authors

Pawan Gupta − *Goddard Space Flight Center, NASA, Greenbelt, Maryland 20771, United States*

Huanxin Zhang − *Department of Chemical and Biochemical Engineering, Iowa Technology Institute, Center for Global and Regional Environmental Research, The University of Iowa, Iowa City, Iowa 52242, United States*

Jun Wang − *Department of Chemical and Biochemical Engineering, Iowa Technology Institute, Center for Global and Regional Environmental Research, The University of Iowa, Iowa City, Iowa 52242, United States;* orcid.org/0000-0002-7334-0490

Complete contact information is available at: https://pubs.acs.org/10.1021/acsestair.4c00120

Author Contributions

The manuscript was written through contributions of all authors. All authors have given approval to the final version of the manuscript.

Notes

The authors declare no competing financial interest.

■ ACKNOWLEDGMENTS

We acknowledge the funding from NASA Grants 80NSSC19M0154 and 80NSSC21K0428. A version of this work was previously presented as a poster at the IGC10 meeting. We thank the NASA CAN award, the HAQAST grant, and the helpful discussion in the HAQAST Tiger Team. We thank the PIs of the eight AERONET sites in Alaska that we used in this work. We thank the Alaska Department of Environmental Conservation (DEC) for providing the data of surface $PM_{2.5}$ measurements.

■ ABBREVIATIONS

AOD = aerosol optical depth
$PM_{2.5}$ = particulate matter with diameter < 2.5μm
$PM_{2.5,SAT}$ = $PM_{2.5}$ derived by η'_{obs} and satellite AOD
CF = conversion factor for PurpleAir $PM_{2.5}$ product
GC = GEOS-Chem
η = conversion factor that converts AOD to surface $PM_{2.5}$ ($\eta = \frac{\text{surface } PM_{2.5}}{\text{AOD}}$)
η_{GC} = η calculated from GEOS-Chem model simulated AOD and surface $PM_{2.5}$
$\eta_{GC,surface}$ = η_{GC} based GEOS-Chem model simulation that injects wildfire emission at the surface layer
$\eta_{GC,35/65}$ = η_{GC} based GEOS-Chem model simulation that injects 35 and 65% of wildfire emissions in free troposphere and within PBL
η_{obs} = η calculated from observed AOD and surface $PM_{2.5}$
η'_{obs} = η calculated based on median value of η_{obs} in various AOD ranges[87]
f_{PBL} = ratio of aerosol optical depth within PBL versus in the total column

■ REFERENCES

(1) Wang, J.; Christopher, S. A.; Nair, U. S.; Reid, J. S.; Prins, E. M.; Szykman, J.; Hand, J. L. Mesoscale Modeling of Central American Smoke Transport to the United States: 1. "Top-down" Assessment of Emission Strength and Diurnal Variation Impacts. *Journal of Geophysical Research: Atmospheres* **2006**, *111* (D5), D05S17.

(2) Val Martín, M.; Honrath, R. E.; Owen, R. C.; Pfister, G.; Fialho, P.; Barata, F. Significant Enhancements of Nitrogen Oxides, Black Carbon, and Ozone in the North Atlantic Lower Free Troposphere Resulting from North American Boreal Wildfires. *Journal of Geophysical Research: Atmospheres* **2006**, *111* (D23), D23S60.

(3) Park, R. J.; Jacob, D. J.; Logan, J. A. Fire and Biofuel Contributions to Annual Mean Aerosol Mass Concentrations in the United States. *Atmospheric Environment* **2007**, *41* (35), 7389−7400.

(4) Yokelson, R. J.; Crounse, J. D.; DeCarlo, P. F.; Karl, T.; Urbanski, S.; Atlas, E.; Campos, T.; Shinozuka, Y.; Kapustin, V.; Clarke, A. D.; Weinheimer, A.; Knapp, D. J.; Montzka, D. D.; Holloway, J.; Weibring, P.; Flocke, F.; Zheng, W.; Toohey, D.; Wennberg, P. O.; Wiedinmyer, C.; Mauldin, L.; Fried, A.; Richter, D.; Walega, J.; Jimenez, J. L.; Adachi, K.; Buseck, P. R.; Hall, S. R.; Shetter, R. Emissions from Biomass Burning in the Yucatan. *Atmospheric Chemistry and Physics* **2009**, *9* (15), 5785−5812.

(5) Cohen, A. J.; Brauer, M.; Burnett, R.; Anderson, H. R.; Frostad, J.; Estep, K.; Balakrishnan, K.; Brunekreef, B.; Dandona, L.; Dandona, R.; Feigin, V.; Freedman, G.; Hubbell, B.; Jobling, A.; Kan, H.; Knibbs, L.;

Liu, Y.; Martin, R.; Morawska, L.; Pope, C. A.; Shin, H.; Straif, K.; Shaddick, G.; Thomas, M.; van Dingenen, R.; van Donkelaar, A.; Vos, T.; Murray, C. J. L.; Forouzanfar, M. H. Estimates and 25-Year Trends of the Global Burden of Disease Attributable to Ambient Air Pollution: An Analysis of Data from the Global Burden of Diseases Study 2015. *Lancet* **2017**, *389* (10082), 1907−1918.

(6) Lim, S. S.; Vos, T.; Flaxman, A. D.; Danaei, G.; Shibuya, K.; Adair-Rohani, H.; Amann, M.; Anderson, H. R.; Andrews, K. G.; Aryee, M.; Atkinson, C.; Bacchus, L. J.; Bahalim, A. N.; Balakrishnan, K.; Balmes, J.; Barker-Collo, S.; Baxter, A.; Bell, M. L.; Blore, J. D.; Blyth, F.; Bonner, C.; Borges, G.; Bourne, R.; Boussinesq, M.; Brauer, M.; Brooks, P.; Bruce, N. G.; Brunekreef, B.; Bryan-Hancock, C.; Bucello, C.; Buchbinder, R.; Bull, F.; Burnett, R. T.; Byers, T. E.; Calabria, B.; Carapetis, J.; Carnahan, E.; Chafe, Z.; Charlson, F.; Chen, H.; Chen, J. S.; Cheng, A. T.-A.; Child, J. C.; Cohen, A.; Colson, K. E.; Cowie, B. C.; Darby, S.; Darling, S.; Davis, A.; Degenhardt, L.; Dentener, F.; Des Jarlais, D. C.; Devries, K.; Dherani, M.; Ding, E. L.; Dorsey, E. R.; Driscoll, T.; Edmond, K.; Ali, S. E.; Engell, R. E.; Erwin, P. J.; Fahimi, S.; Falder, G.; Farzadfar, F.; Ferrari, A.; Finucane, M. M.; Flaxman, S.; Fowkes, F. G. R.; Freedman, G.; Freeman, M. K.; Gakidou, E.; Ghosh, S.; Giovannucci, E.; Gmel, G.; Graham, K.; Grainger, R.; Grant, B.; Gunnell, D.; Gutierrez, H. R.; Hall, W.; Hoek, H. W.; Hogan, A.; Hosgood, H. D.; Hoy, D.; Hu, H.; Hubbell, B. J.; Hutchings, S. J.; Ibeanusi, S. E.; Jacklyn, G. L.; Jasrasaria, R.; Jonas, J. B.; Kan, H.; Kanis, J. A.; Kassebaum, N.; Kawakami, N.; Khang, Y.-H.; Khatibzadeh, S.; Khoo, J.-P.; Kok, C.; Laden, F.; Lalloo, R.; Lan, Q.; Lathlean, T.; Leasher, J. L.; Leigh, J.; Li, Y.; Lin, J. K.; Lipshultz, S. E.; London, S.; Lozano, R.; Lu, Y.; Mak, J.; Malekzadeh, R.; Mallinger, L.; Marcenes, W.; March, L.; Marks, R.; Martin, R.; McGale, P.; McGrath, J.; Mehta, S.; Mensah, G. A.; Merriman, T. R.; Micha, R.; Michaud, C.; Mishra, V.; Hanafiah, K. M.; Mokdad, A. A.; Morawska, L.; Mozaff arian, D.; Murphy, T.; Naghavi, M.; Neal, B.; Nelson, P. K.; Nolla, J. M.; Norman, R.; Olives, C.; Omer, S. B.; Orchard, J.; Osborne, R.; Ostro, B.; Page, A.; Pandey, K. D.; Parry, C. D. H.; Passmore, E.; Patra, J.; Pearce, N.; Pelizzari, P. M.; Petzold, M.; Phillips, M. R.; Pope, D.; Pope, C. A., III; Powles, J.; Rao, M.; Razavi, H.; Rehfuess, E. A.; Rehm, J. T.; Ritz, B.; Rivara, F. P.; Roberts, T.; Robinson, C.; Rodriguez-Portales, J. A.; Romieu, I.; Room, R.; Rosenfeld, L. C.; Roy, A.; Rushton, L.; Salomon, J. A.; Sampson, U.; Sanchez-Riera, L.; Sanman, E.; Sapkota, A.; Seedat, S.; Shi, P.; Shield, K.; Shivakoti, R.; Singh, G. M.; Sleet, D. A.; Smith, E.; Smith, K. R.; Stapelberg, N. J. C.; Steenland, K.; Stöckl, H.; Stovner, L. J.; Straif, K.; Straney, L.; Thurston, G. D.; Tran, J. H.; Van Dingenen, R.; van Donkelaar, A.; Veerman, J. L.; Vijayakumar, L.; Weintraub, R.; Weissman, M. M.; White, R. A.; Whiteford, H.; Wiersma, S. T.; Wilkinson, J. D.; Williams, H. C.; Williams, W.; Wilson, N.; Woolf, A. D.; Yip, P.; Zielinski, J. M.; Lopez, A. D.; Murray, C. J. L.; Ezzati, M.; AlMazroa, M. A.; Memish, Z. A. A Comparative Risk Assessment of Burden of Disease and Injury Attributable to 67 Risk Factors and Risk Factor Clusters in 21 Regions, 1990−2010: A Systematic Analysis for the Global Burden of Disease Study 2010. *Lancet* **2012**, *380* (9859), 2224−2260.

(7) Kelly, R.; Chipman, M. L.; Higuera, P. E.; Stefanova, I.; Brubaker, L. B.; Hu, F. S. Recent Burning of Boreal Forests Exceeds Fire Regime Limits of the Past 10,000 Years. *Proc. Natl. Acad. Sci. U.S.A.* **2013**, *110* (32), 13055−13060.

(8) Yue, X.; Mickley, L. J.; Logan, J. A.; Kaplan, J. O. Ensemble Projections of Wildfire Activity and Carbonaceous Aerosol Concentrations over the Western United States in the Mid-21st Century. *Atmospheric Environment* **2013**, *77*, 767−780.

(9) Yue, X.; Mickley, L. J.; Logan, J. A. Projection of Wildfire Activity in Southern California in the Mid-Twenty-First Century. *Clim Dyn* **2014**, *43* (7), 1973−1991.

(10) Dennison, P. E.; Brewer, S. C.; Arnold, J. D.; Moritz, M. A. Large Wildfire Trends in the Western United States, 1984−2011. *Geophysical Research Letters* **2014**, *41* (8), 2928−2933.

(11) Abatzoglou, J. T.; Williams, A. P. Impact of Anthropogenic Climate Change on Wildfire across Western US Forests. *Proc. Natl. Acad. Sci. U. S. A.* **2016**, *113* (42), 11770−11775.

(12) Ford, B.; Val Martin, M.; Zelasky, S. E.; Fischer, E. V.; Anenberg, S. C.; Heald, C. L.; Pierce, J. R. Future Fire Impacts on Smoke Concentrations, Visibility, and Health in the Contiguous United States. *GeoHealth* **2018**, *2* (8), 229−247.

(13) Zhao, T.; Mao, J.; Simpson, W. R.; De Smedt, I.; Zhu, L.; Hanisco, T. F.; Wolfe, G. M.; St. Clair, J. M.; González Abad, G.; Nowlan, C. R.; Barletta, B.; Meinardi, S.; Blake, D. R.; Apel, E. C.; Hornbrook, R. S. Source and Variability of Formaldehyde (HCHO) at Northern High Latitudes: An Integrated Satellite, Aircraft, and Model Study. *Atmos. Chem. Phys.* **2022**, *22* (11), 7163−7178.

(14) Gupta, P.; Christopher, S. A.; Wang, J.; Gehrig, R.; Lee, Y.; Kumar, N. Satellite Remote Sensing of Particulate Matter and Air Quality Assessment over Global Cities. *Atmos. Environ.* **2006**, *40* (30), 5880−5892.

(15) Gupta, P.; Christopher, S. A.; Box, M. A.; Box, G. P. Multi Year Satellite Remote Sensing of Particulate Matter Air Quality over Sydney, Australia. *International Journal of Remote Sensing* **2007**, *28* (20), 4483−4498.

(16) Wang, J.; Christopher, S. A. Intercomparison between Satellite-Derived Aerosol Optical Thickness and PM2.5 Mass: Implications for Air Quality Studies. *Geophysical Research Letters* **2003**, *30* (21), 2095.

(17) Liu, H.; Remer, L. A.; Huang, J.; Huang, H.-C.; Kondragunta, S.; Laszlo, I.; Oo, M.; Jackson, J. M. Preliminary Evaluation of S-NPP VIIRS Aerosol Optical Thickness. *Journal of Geophysical Research: Atmospheres* **2014**, *119* (7), 3942−3962.

(18) Wang, J.; Aegerter, C.; Xu, X.; Szykman, J. J. Potential Application of VIIRS Day/Night Band for Monitoring Nighttime Surface PM 2.5 Air Quality from Space. *Atmospheric Environment* **2016**, *124*, 55−63.

(19) Zhou, M.; Wang, J.; Chen, X.; Xu, X.; Colarco, P. R.; Miller, S. D.; Reid, J. S.; Kondragunta, S.; Giles, D. M.; Holben, B. Nighttime Smoke Aerosol Optical Depth over U.S. Rural Areas: First Retrieval from VIIRS Moonlight Observations. *Remote Sensing of Environment* **2021**, *267*, No. 112717.

(20) Gupta, P.; Christopher, S. A. Particulate Matter Air Quality Assessment Using Integrated Surface, Satellite, and Meteorological Products: Multiple Regression Approach. *Journal of Geophysical Research: Atmospheres* **2009**, *114* (D14), D14205.

(21) Liu, Y.; Paciorek, C. J.; Koutrakis, P. Estimating Regional Spatial and Temporal Variability of PM2.5 Concentrations Using Satellite Data, Meteorology, and Land Use Information. *Environ. Health Perspect* **2009**, *117* (6), 886−892.

(22) Goldberg, D. L.; Gupta, P.; Wang, K.; Jena, C.; Zhang, Y.; Lu, Z.; Streets, D. G. Using Gap-Filled MAIAC AOD and WRF-Chem to Estimate Daily PM2.5 Concentrations at 1 km Resolution in the Eastern United States. *Atmospheric Environment* **2019**, *199*, 443−452.

(23) Hu, X.; Waller, L. A.; Al-Hamdan, M. Z.; Crosson, W. L.; Estes, M. G.; Estes, S. M.; Quattrochi, D. A.; Sarnat, J. A.; Liu, Y. Estimating Ground-Level PM2.5 Concentrations in the Southeastern U.S. Using Geographically Weighted Regression. *Environmental Research* **2013**, *121*, 1−10.

(24) Ma, Z.; Hu, X.; Huang, L.; Bi, J.; Liu, Y. Estimating Ground-Level PM2.5 in China Using Satellite Remote Sensing. *Environ. Sci. Technol.* **2014**, *48* (13), 7436−7444.

(25) Zou, B.; Pu, Q.; Bilal, M.; Weng, Q.; Zhai, L.; Nichol, J. E. High-Resolution Satellite Mapping of Fine Particulates Based on Geographically Weighted Regression. *IEEE Geoscience and Remote Sensing Letters* **2016**, *13* (4), 495−499.

(26) van Donkelaar, A.; Martin, R. V.; Brauer, M.; Hsu, N. C.; Kahn, R. A.; Levy, R. C.; Lyapustin, A.; Sayer, A. M.; Winker, D. M. Global Estimates of Fine Particulate Matter Using a Combined Geophysical-Statistical Method with Information from Satellites, Models, and Monitors. *Environ. Sci. Technol.* **2016**, *50* (7), 3762−3772.

(27) Zhang, H.; Kondragunta, S. Daily and Hourly Surface PM2.5 Estimation From Satellite AOD. *Earth and Space Science* **2021**, *8* (3), No. e2020EA001599.

(28) Gupta, P.; Christopher, S. A. Particulate Matter Air Quality Assessment Using Integrated Surface, Satellite, and Meteorological

https://doi.org/10.1021/acsestair.4c00120
ACS EST Air 2024, 1, 1164−1176

Products: 2. A Neural Network Approach. *Journal of Geophysical Research: Atmospheres* **2009**, *114* (D20), D20205.
(29) Nabavi, S. O.; Haimberger, L.; Abbasi, E. Assessing PM2.5 Concentrations in Tehran, Iran, from Space Using MAIAC, Deep Blue, and Dark Target AOD and Machine Learning Algorithms. *Atmospheric Pollution Research* **2019**, *10* (3), 889−903.
(30) Hu, X.; Belle, J. H.; Meng, X.; Wildani, A.; Waller, L. A.; Strickland, M. J.; Liu, Y. Estimating PM2.5 Concentrations in the Conterminous United States Using the Random Forest Approach. *Environ. Sci. Technol.* **2017**, *51* (12), 6936−6944.
(31) Liu, Y.; Park, R. J.; Jacob, D. J.; Li, Q.; Kilaru, V.; Sarnat, J. A. Mapping Annual Mean Ground-Level PM2.5 Concentrations Using Multiangle Imaging Spectroradiometer Aerosol Optical Thickness over the Contiguous United States. *Journal of Geophysical Research: Atmospheres* **2004**, *109* (D22), D22206.
(32) van Donkelaar, A.; Martin, R. V.; Park, R. J. Estimating Ground-Level PM2.5 Using Aerosol Optical Depth Determined from Satellite Remote Sensing. *Journal of Geophysical Research: Atmospheres* **2006**, *111* (D21), D21201.
(33) van Donkelaar, A.; Martin, R. V.; Brauer, M.; Kahn, R.; Levy, R.; Verduzco, C.; Villeneuve, P. J. Global Estimates of Ambient Fine Particulate Matter Concentrations from Satellite-Based Aerosol Optical Depth: Development and Application. *Environ. Health Perspect* **2010**, *118* (6), 847−855.
(34) Drury, E.; Jacob, D. J.; Spurr, R. J. D.; Wang, J.; Shinozuka, Y.; Anderson, B. E.; Clarke, A. D.; Dibb, J.; McNaughton, C.; Weber, R. Synthesis of Satellite (MODIS), Aircraft (ICARTT), and Surface (IMPROVE, EPA-AQS, AERONET) Aerosol Observations over Eastern North America to Improve MODIS Aerosol Retrievals and Constrain Surface Aerosol Concentrations and Sources. *Journal of Geophysical Research: Atmospheres* **2010**, *115* (D14), D14204.
(35) Wang, J.; Xu, X.; Spurr, R.; Wang, Y.; Drury, E. Improved Algorithm for MODIS Satellite Retrievals of Aerosol Optical Thickness over Land in Dusty Atmosphere: Implications for Air Quality Monitoring in China. *Remote Sensing of Environment* **2010**, *114* (11), 2575−2583.
(36) Ye, X.; Arab, P.; Ahmadov, R.; James, E.; Grell, G. A.; Pierce, B.; Kumar, A.; Makar, P.; Chen, J.; Davignon, D.; Carmichael, G. R.; Ferrada, G.; McQueen, J.; Huang, J.; Kumar, R.; Emmons, L.; Herron-Thorpe, F. L.; Parrington, M.; Engelen, R.; Peuch, V.-H.; da Silva, A.; Soja, A.; Gargulinski, E.; Wiggins, E.; Hair, J. W.; Fenn, M.; Shingler, T.; Kondragunta, S.; Lyapustin, A.; Wang, Y.; Holben, B.; Giles, D. M.; Saide, P. E. Evaluation and Intercomparison of Wildfire Smoke Forecasts from Multiple Modeling Systems for the 2019 Williams Flats Fire. *Atmospheric Chemistry and Physics* **2021**, *21* (18), 14427−14469.
(37) Paugam, R.; Wooster, M.; Freitas, S.; Val Martin, M. A Review of Approaches to Estimate Wildfire Plume Injection Height within Large-Scale Atmospheric Chemical Transport Models. *Atmospheric Chemistry and Physics* **2016**, *16* (2), 907−925.
(38) van Donkelaar, A.; Martin, R. V.; Spurr, R. J. D.; Drury, E.; Remer, L. A.; Levy, R. C.; Wang, J. Optimal Estimation for Global Ground-Level Fine Particulate Matter Concentrations. *Journal of Geophysical Research: Atmospheres* **2013**, *118* (11), 5621−5636.
(39) van Donkelaar, A.; Martin, R. V.; Levy, R. C.; da Silva, A. M.; Krzyzanowski, M.; Chubarova, N. E.; Semutnikova, E.; Cohen, A. J. Satellite-Based Estimates of Ground-Level Fine Particulate Matter during Extreme Events: A Case Study of the Moscow Fires in 2010. *Atmospheric Environment* **2011**, *45* (34), 6225−6232.
(40) Zhong, Q.; Schutgens, N.; van der Werf, G.; van Noije, T.; Tsigaridis, K.; Bauer, S. E.; Mielonen, T.; Kirkevåg, A.; Seland, Ø.; Kokkola, H.; Checa-Garcia, R.; Neubauer, D.; Kipling, Z.; Matsui, H.; Ginoux, P.; Takemura, T.; Le Sager, P.; Rémy, S.; Bian, H.; Chin, M.; Zhang, K.; Zhu, J.; Tsyro, S. G.; Curci, G.; Protonotariou, A.; Johnson, B.; Penner, J. E.; Bellouin, N.; Skeie, R. B.; Myhre, G. Satellite-Based Evaluation of AeroCom Model Bias in Biomass Burning Regions. *Atmospheric Chemistry and Physics* **2022**, *22*, 11009.
(41) Holben, B. N.; Tanré, D.; Smirnov, A.; Eck, T. F.; Slutsker, I.; Abuhassan, N.; Newcomb, W. W.; Schafer, J. S.; Chatenet, B.; Lavenu, F.; Kaufman, Y. J.; Castle, J. V.; Setzer, A.; Markham, B.; Clark, D.; Frouin, R.; Halthore, R.; Karneli, A.; O'Neill, N. T.; Pietras, C.; Pinker, R. T.; Voss, K.; Zibordi, G. An Emerging Ground-Based Aerosol Climatology: Aerosol Optical Depth from AERONET. *Journal of Geophysical Research: Atmospheres* **2001**, *106* (D11), 12067−12097.
(42) Eck; Holben; Reid; Dubovik; Smirnov; O'Neill; Slutsker; Kinne. Wavelength Dependence of the Optical Depth of Biomass Burning, Urban, and Desert Dust Aerosols. *Journal of Geophysical Research: Atmospheres* **1999**, *104* (D24), 31333−31349.
(43) Sawyer, V.; Levy, R. C.; Mattoo, S.; Cureton, G.; Shi, Y.; Remer, L. A. Continuing the MODIS Dark Target Aerosol Time Series with VIIRS. *Remote Sensing* **2020**, *12*, 308.
(44) Levy, R. C.; Munchak, L. A.; Mattoo, S.; Patadia, F.; Remer, L. A.; Holz, R. E. Towards a Long-Term Global Aerosol Optical Depth Record: Applying a Consistent Aerosol Retrieval Algorithm to MODIS and VIIRS-Observed Reflectance. *Atmospheric Measurement Techniques* **2015**, *8* (10), 4083−4110.
(45) Sayer, A. M.; Hsu, N. C.; Lee, J.; Bettenhausen, C.; Kim, W. V.; Smirnov, A. Satellite Ocean Aerosol Retrieval (SOAR) Algorithm Extension to S-NPP VIIRS as Part of the "Deep Blue" Aerosol Project. *J. Geophys Res. Atmos* **2018**, *123* (1), 380−400.
(46) Gupta, P.; Remer, L. A.; Patadia, F.; Levy, R. C.; Christopher, S. A. High-Resolution Gridded Level 3 Aerosol Optical Depth Data from MODIS. *Remote Sensing* **2020**, *12* (17), 2847.
(47) Chudnovsky, A.; Tang, C.; Lyapustin, A.; Wang, Y.; Schwartz, J.; Koutrakis, P. A Critical Assessment of High-Resolution Aerosol Optical Depth Retrievals for Fine Particulate Matter Predictions. *Atmos. Chem. Phys.* **2013**, *13* (21), 10907−10917.
(48) Jin, Q.; Crippa, P.; Pryor, S. C. Spatial Characteristics and Temporal Evolution of the Relationship between PM2.5 and Aerosol Optical Depth over the Eastern USA during 2003−2017. *Atmospheric Environment* **2020**, *239*, No. 117718.
(49) van Donkelaar, A.; Martin, R. V.; Brauer, M.; Boys, B. L. Use of Satellite Observations for Long-Term Exposure Assessment of Global Concentrations of Fine Particulate Matter. *Environ. Health Perspect.* **2015**, *123* (2), 135−143.
(50) Jackson, J. M.; Liu, H.; Laszlo, I.; Kondragunta, S.; Remer, L. A.; Huang, J.; Huang, H.-C. Suomi-NPP VIIRS Aerosol Algorithms and Data Products. *Journal of Geophysical Research: Atmospheres* **2013**, *118* (22), 12673−12689.
(51) Levy, R. C.; Mattoo, S.; Munchak, L. A.; Remer, L. A.; Sayer, A. M.; Patadia, F.; Hsu, N. C. The Collection 6 MODIS Aerosol Products over Land and Ocean. *Atmospheric Measurement Techniques* **2013**, *6* (11), 2989−3034.
(52) Hsu, N. C.; Jeong, M.-J.; Bettenhausen, C.; Sayer, A. M.; Hansell, R.; Seftor, C. S.; Huang, J.; Tsay, S.-C. Enhanced Deep Blue Aerosol Retrieval Algorithm: The Second Generation. *Journal of Geophysical Research: Atmospheres* **2013**, *118* (16), 9296−9315.
(53) McPhetres, A.; Aggarwal, S. An Evaluation of MODIS-Retrieved Aerosol Optical Depth over AERONET Sites in Alaska. *Remote Sensing* **2018**, *10* (9), 1384.
(54) Sayer, A. M.; Hsu, N. C.; Lee, J.; Kim, W. V.; Dutcher, S. T. Validation, Stability, and Consistency of MODIS Collection 6.1 and VIIRS Version 1 Deep Blue Aerosol Data Over Land. *Journal of Geophysical Research: Atmospheres* **2019**, *124* (8), 4658−4688.
(55) Petrenko, M.; Ichoku, C.; Leptoukh, G. Multi-Sensor Aerosol Products Sampling System (MAPSS). *Atmospheric Measurement Techniques* **2012**, *5* (5), 913−926.
(56) Winker, D. M.; Vaughan, M. A.; Omar, A.; Hu, Y.; Powell, K. A.; Liu, Z.; Hunt, W. H.; Young, S. A. Overview of the CALIPSO Mission and CALIOP Data Processing Algorithms. *Journal of Atmospheric and Oceanic Technology* **2009**, *26* (11), 2310−2323.
(57) Tackett, J. L.; Winker, D. M.; Getzewich, B. J.; Vaughan, M. A.; Young, S. A.; Kar, J. CALIPSO Lidar Level 3 Aerosol Profile Product: Version 3 Algorithm Design. *Atmospheric Measurement Techniques* **2018**, *11* (7), 4129−4152.
(58) Kim, M.-H.; Omar, A. H.; Tackett, J. L.; Vaughan, M. A.; Winker, D. M.; Trepte, C. R.; Hu, Y.; Liu, Z.; Poole, L. R.; Pitts, M. C.; Kar, J.; Magill, B. E. The CALIPSO Version 4 Automated Aerosol

https://doi.org/10.1021/acsestair.4c00120
ACS EST Air 2024, 1, 1164−1176

Classification and Lidar Ratio Selection Algorithm. *Atmospheric Measurement Techniques* **2018**, *11* (11), 6107−6135.
(59) Zhao, T.; Mao, J.; Ayazpour, Z.; González Abad, G.; Nowlan, C.; Zheng, Y. Interannual Variability of Summertime Formaldehyde (HCHO) Vertical Column Density and Its Main Drivers in Northern High Latitudes. *Atmospheric Chemistry and Physics* **2024**, *24*, 6105−6121.
(60) Rienecker, M. M.; Suarez, M. J.; Gelaro, R.; Todling, R.; Bacmeister, J.; Liu, E.; Bosilovich, M. G.; Schubert, S. D.; Takacs, L.; Kim, G.-K.; Bloom, S.; Chen, J.; Collins, D.; Conaty, A.; da Silva, A.; Gu, W.; Joiner, J.; Koster, R. D.; Lucchesi, R.; Molod, A.; Owens, T.; Pawson, S.; Pegion, P.; Redder, C. R.; Reichle, R.; Robertson, F. R.; Ruddick, A. G.; Sienkiewicz, M.; Woollen, J. MERRA: NASA's Modern-Era Retrospective Analysis for Research and Applications. *J. Climate* **2011**, *24* (14), 3624−3648.
(61) Park, R. J.; Jacob, D. J.; Field, B. D.; Yantosca, R. M.; Chin, M. Natural and Transboundary Pollution Influences on Sulfate-Nitrate-Ammonium Aerosols in the United States: Implications for Policy. *Journal of Geophysical Research: Atmospheres* **2004**, *109* (D15), D15204.
(62) Mao, J.; Jacob, D. J.; Evans, M. J.; Olson, J. R.; Ren, X.; Brune, W. H.; Clair, J. M. S.; Crounse, J. D.; Spencer, K. M.; Beaver, M. R.; Wennberg, P. O.; Cubison, M. J.; Jimenez, J. L.; Fried, A.; Weibring, P.; Walega, J. G.; Hall, S. R.; Weinheimer, A. J.; Cohen, R. C.; Chen, G.; Crawford, J. H.; McNaughton, C.; Clarke, A. D.; Jaeglé, L.; Fisher, J. A.; Yantosca, R. M.; Le Sager, P.; Carouge, C. Chemistry of Hydrogen Oxide Radicals (HO_x) in the Arctic Troposphere in Spring. *Atmospheric Chemistry and Physics* **2010**, *10* (13), 5823−5838.
(63) Mao, J.; Paulot, F.; Jacob, D. J.; Cohen, R. C.; Crounse, J. D.; Wennberg, P. O.; Keller, C. A.; Hudman, R. C.; Barkley, M. P.; Horowitz, L. W. Ozone and Organic Nitrates over the Eastern United States: Sensitivity to Isoprene Chemistry. *Journal of Geophysical Research: Atmospheres* **2013**, *118* (19), 11256−11268.
(64) Lin, J.-T.; McElroy, M. B.Impacts of Boundary Layer Mixing on Pollutant Vertical Profiles in the Lower Troposphere: Implications to Satellite Remote Sensing.*Atmos. Environ.* 2010441417261739.
(65) Guenther, A.; Hewitt, C. N.; Erickson, D.; Fall, R.; Geron, C.; Graedel, T.; Harley, P.; Klinger, L.; Lerdau, M.; McKay, W. A.; Pierce, T.; Scholes, B.; Steinbrecher, R.; Tallamraju, R.; Taylor, J.; Zimmerman, P. A Global-Model of Natural Volatile Organic-Compound Emissions. *Journal of Geophysical Research-Atmospheres* **1995**, *100* (D5), 8873−8892.
(66) Guenther, A.; Karl, T.; Harley, P.; Wiedinmyer, C.; Palmer, P. I.; Geron, C. Estimates of Global Terrestrial Isoprene Emissions Using MEGAN (Model of Emissions of Gases and Aerosols from Nature). *Atmos. Chem. Phys.* **2006**, *6*, 3181−3210.
(67) Guenther, A. B.; Jiang, X.; Heald, C. L.; Sakulyanontvittaya, T.; Duhl, T.; Emmons, L. K.; Wang, X. The Model of Emissions of Gases and Aerosols from Nature Version 2.1 (MEGAN2.1): An Extended and Updated Framework for Modeling Biogenic Emissions. *Geoscientific Model Development* **2012**, *5* (6), 1471−1492.
(68) Hoesly, R. M.; Smith, S. J.; Feng, L.; Klimont, Z.; Janssens-Maenhout, G.; Pitkanen, T.; Seibert, J. J.; Vu, L.; Andres, R. J.; Bolt, R. M.; Bond, T. C.; Dawidowski, L.; Kholod, N.; Kurokawa, J.; Li, M.; Liu, L.; Lu, Z.; Moura, M. C. P.; O'Rourke, P. R.; Zhang, Q. Historical (1750−2014) Anthropogenic Emissions of Reactive Gases and Aerosols from the Community Emissions Data System (CEDS). *Geoscientific Model Development* **2018**, *11* (1), 369−408.
(69) McDuffie, E. E.; Smith, S. J.; O'Rourke, P.; Tibrewal, K.; Venkataraman, C.; Marais, E. A.; Zheng, B.; Crippa, M.; Brauer, M.; Martin, R. V. A Global Anthropogenic Emission Inventory of Atmospheric Pollutants from Sector- and Fuel-Specific Sources (1970−2017): An Application of the Community Emissions Data System (CEDS). *Earth System Science Data* **2020**, *12* (4), 3413−3442.
(70) Giglio, L.; Randerson, J. T.; van der Werf, G. R. Analysis of Daily, Monthly, and Annual Burned Area Using the Fourth-Generation Global Fire Emissions Database (GFED4). *Journal of Geophysical Research: Biogeosciences* **2013**, *118* (1), 317−328.
(71) van der Werf, G. R.; Randerson, J. T.; Giglio, L.; van Leeuwen, T. T.; Chen, Y.; Rogers, B. M.; Mu, M.; van Marle, M. J. E.; Morton, D. C.; Collatz, G. J.; Yokelson, R. J.; Kasibhatla, P. S. Global Fire Emissions Estimates during 1997−2016. *Earth Syst. Sci. Data* **2017**, *9* (2), 697−720.
(72) Jaeglé, L.; Quinn, P. K.; Bates, T. S.; Alexander, B.; Lin, J.-T. Global Distribution of Sea Salt Aerosols: New Constraints from in Situ and Remote Sensing Observations. *Atmospheric Chemistry and Physics* **2011**, *11* (7), 3137−3157.
(73) Castell, N.; Dauge, F. R.; Schneider, P.; Vogt, M.; Lerner, U.; Fishbain, B.; Broday, D.; Bartonova, A. Can Commercial Low-Cost Sensor Platforms Contribute to Air Quality Monitoring and Exposure Estimates? *Environ. Int.* **2017**, *99*, 293−302.
(74) Magi, B. I.; Cupini, C.; Francis, J.; Green, M.; Hauser, C. Evaluation of PM2.5 Measured in an Urban Setting Using a Low-Cost Optical Particle Counter and a Federal Equivalent Method Beta Attenuation Monitor. *Aerosol Science and Technology* **2020**, *54* (2), 147−159.
(75) deSouza, P.; Kinney, P. L. On the Distribution of Low-Cost PM2.5 Sensors in the US: Demographic and Air Quality Associations. *J. Expo Sci. Environ. Epidemiol* **2021**, *31* (3), 514−524.
(76) Barkjohn, K. K.; Gantt, B.; Clements, A. L. Development and Application of a United States-Wide Correction for $PM_{2.5}$ Data Collected with the PurpleAir Sensor. *Atmospheric Measurement Techniques* **2021**, *14* (6), 4617−4637.
(77) Jaffe, D. A.; Miller, C.; Thompson, K.; Finley, B.; Nelson, M.; Ouimette, J.; Andrews, E. An Evaluation of the U.S. EPA's Correction Equation for PurpleAir Sensor Data in Smoke, Dust, and Wintertime Urban Pollution Events. *Atmospheric Measurement Techniques* **2023**, *16* (5), 1311−1322.
(78) Liu, Y.; Sarnat, J. A.; Kilaru, V.; Jacob, D. J.; Koutrakis, P. Estimating Ground-Level PM2.5 in the Eastern United States Using Satellite Remote Sensing. *Environ. Sci. Technol.* **2005**, *39* (9), 3269−3278.
(79) Hu, X.; Waller, L. A.; Al-Hamdan, M. Z.; Crosson, W. L.; Estes, M. G.; Estes, S. M.; Quattrochi, D. A.; Sarnat, J. A.; Liu, Y. Estimating Ground-Level PM2.5 Concentrations in the Southeastern U.S. Using Geographically Weighted Regression. *Environmental Research* **2013**, *121*, 1−10.
(80) Geng, G.; Zhang, Q.; Martin, R. V.; van Donkelaar, A.; Huo, H.; Che, H.; Lin, J.; He, K. Estimating Long-Term PM2.5 Concentrations in China Using Satellite-Based Aerosol Optical Depth and a Chemical Transport Model. *Remote Sensing of Environment* **2015**, *166*, 262−270.
(81) Geng, G.; Murray, N. L.; Tong, D.; Fu, J. S.; Hu, X.; Lee, P.; Meng, X.; Chang, H. H.; Liu, Y. Satellite-Based Daily PM2.5 Estimates During Fire Seasons in Colorado. *Journal of Geophysical Research: Atmospheres* **2018**, *123* (15), 8159−8171.
(82) Amiridis, V.; Giannakaki, E.; Balis, D. S.; Gerasopoulos, E.; Pytharoulis, I.; Zanis, P.; Kazadzis, S.; Melas, D.; Zerefos, C. Smoke Injection Heights from Agricultural Burning in Eastern Europe as Seen by CALIPSO. *Atmospheric Chemistry and Physics* **2010**, *10* (23), 11567−11576.
(83) Vinjamuri, K. S.; Mhawish, A.; Banerjee, T.; Sorek-Hamer, M.; Broday, D. M.; Mall, R. K.; Latif, M. T. Vertical Distribution of Smoke Aerosols over Upper Indo-Gangetic Plain. *Environmental Pollution* **2020**, *257*, No. 113377.
(84) Ye, X.; Saide, P. E.; Hair, J.; Fenn, M.; Shingler, T.; Soja, A.; Gargulinski, E.; Wiggins, E. Assessing Vertical Allocation of Wildfire Smoke Emissions Using Observational Constraints From Airborne Lidar in the Western U.S. *Journal of Geophysical Research: Atmospheres* **2022**, *127* (21), No. e2022JD036808.
(85) Cheeseman, M.; Ford, B.; Volckens, J.; Lyapustin, A.; Pierce, J. R. The Relationship Between MAIAC Smoke Plume Heights and Surface PM. *Geophysical Research Letters* **2020**, *47* (17), No. e2020GL088949.
(86) Ohneiser, K.; Ansmann, A.; Witthuhn, J.; Deneke, H.; Chudnovsky, A.; Walter, G.; Senf, F. Self-Lofting of Wildfire Smoke in the Troposphere and Stratosphere: Simulations and Space Lidar Observations. *Atmospheric Chemistry and Physics* **2023**, *23* (4), 2901−2925.
(87) Here η_{obs} is computed using weekly satellite AOD and PurpleAir surface $PM_{2.5}$ over the Alaska domain in the 2019 summertime.

https://doi.org/10.1021/acsestair.4c00120
ACS EST Air 2024, 1, 1164−1176